Band structure and Fermi surface of $(Sr_2VO_3)_2Fe_2As_2$ and $(Sr_2ScO_3)_2Fe_2As_2$

Guangtao Wang, Minping Zhang, Lihua Zheng, and Zongxian Yang
College of Physics and Information Engineering, Henan Normal University, Xinxiang, Henan 453007, People's Republic of China
(Received 3 July 2009; revised manuscript received 11 October 2009; published 2 November 2009)

Inspired by the experience in CuO-based superconductor that larger spacing distance between CuO planes induced higher superconductivity transition temperature (T_C), some researchers synthesized $(Sr_2ScO_3)_2Fe_2As_2$ and $(Sr_2VO_3)_2Fe_2As_2$ with the spacing distance between FeAs layers as large as 15.66 Å and found a T_C of 37.2 K in the latter compound. Our density-functional calculations indicate that the ground states of $(Sr_2ScO_3)_2Fe_2As_2$ and $(Sr_2VO_3)_2Fe_2As_2$ are stripe antiferromagnetic and checkerboard antiferromagnetic, respectively. The band structure and Fermi surface of $(Sr_2ScO_3)_2Fe_2As_2$ are similar to those of LaOFeAs, while those of $(Sr_2VO_3)_2Fe_2As_2$ show significant difference. In $(Sr_2VO_3)_2Fe_2As_2$, both Fe 3*d* and V 3*d* states contribute to the Fermi surfaces, which implies that the V 3*d* states may play important roles in the superconductivity.

DOI: 10.1103/PhysRevB.80.184501 PACS number(s): 74.25.Ha, 71.18.+y, 71.20.−b

I. INTRODUCTION

The recent discovery[1] of superconductivity in the FeAs-based compound $LaFeAsO_{1-x}F_x$ with transition temperature T_C=26 K has generated great excitement. Subsequently, other related compounds $LnFeAsO_{1-x}F_x$ (*Ln*=Sm, Nd, and Ce) have been synthesized with T_C ranging from 10 K to as high as 55 K.[2–5] This series of compounds crystallized in ZrCuSiAs structure and have often been abbreviated as FeAs-1111 system. Later, three new series of compounds, such as $A_{1-x}K_xFe_2As_2$ (*A*=Ba, Sr, Ca, and Eu),[6–10] Li_xFeAs,[11–13] and $FeSe_{1-x}$,[14] were reported with their maximum T_C at about 38, 18, and 8 K, respectively.

The common features of the above-mentioned FeAs-based superconductive compounds are that their phases adopt quasi-two-dimensional crystal structures, where superconducting [FeAs] layers are separated by either [LnO], [AO] layers, or Li atomic sheets, which act as "charge reservoir." After analyzing the relationship between the maximum transition temperature T_C and the spacing distance between neighboring FeAs layers (d_{FeAs}), we find an interesting trend that T_C raises with the increase in d_{FeAs} (Li_xFeAs: T_C=18 K, d_{FeAs}=6.4 Å; $A_{1-x}K_xFe_2As_2$: T_C=38 K, d_{FeAs}=6.5 Å; and SmFeAsOF: T_C=55 K, d_{FeAs}=8.7 Å).[2–8,12,13] Such trend has also been revealed in Cu-based superconductor. For the single-layer systems, such as $La_{1-x}Sr_xCuO_4$ and $Bi_2Sr_2CuO_6$, their maximum T_C are about 38 K. Increasing the spacing distance between neighboring CuO layers in double-layer systems, such as $YBa_2Cu_3O_7$ and $Bi_2Sr_2CaCu_2O_8$, their maximum T_C raise up to 92 K. For triple-layer system $Bi_2Sr_2Ca_2Cu_3O_{10}$, its spacing distance further increases, accompanying with a higher T_C of 123 K. Inspired by the experience in CuO-based superconductor, some researchers believed that the larger spacing distance may lead to the higher T_C and they started to look for FeAs-based compounds with larger d_{FeAs}. Indeed, some FeAs-based compounds with d_{FeAs} larger than 15 Å had been fabricated successfully by different groups[15–20] and studied by the first-principles calculations.[21] Among these compounds, $(Sr_2ScO_3)_2Fe_2As_2$ and $(Sr_2VO_3)_2Fe_2As_2$ are isostructural with $(Sr_4Sc_2O_6)Fe_2P_2$ while their electrical resistibility are significantly different. $(Sr_2VO_3)_2Fe_2As_2$ and $(Sr_4Sc_2O_6)Fe_2P_2$ show metallic resistivity[16,20] while $(Sr_2ScO_3)_2Fe_2As_2$ shows insulative resistivity.[17] The other important difference is that $(Sr_2ScO_3)_2Fe_2As_2$ and $(Sr_2VO_3)_2Fe_2As_2$ become superconductor at about 17 and 37.2 K, respectively. However, $(Sr_2ScO_3)_2Fe_2As_2$ does not exhibit any signs of superconductivity down to 1.7 K. Although Shein and Ivanovskii[21] had studied the band structure and Fermi surface (FS) of $(Sr_2ScO_3)_2Fe_2As_2$ and $(Sr_2VO_3)_2Fe_2As_2$ by the first-principles full-potential linearized augmented plane wave (FLAPW)–generalized gradient approximation (GGA) calculations, they only involved the nonmagnetic (NM) and ferromagnetic (FM) states, without the antiferromagnetic (AF) state. However, it is well known that the ground states of both LaOFeAs and $BaFe_2As_2$ are stripe antiferromagnetism. Therefore, it is great in need to study the antiferromagnetic state for both $(Sr_2ScO_3)_2Fe_2As_2$ and $(Sr_2VO_3)_2Fe_2As_2$ in the present work.

II. METHOD AND DETAILS

The calculations are performed with the BSTATE (Ref. 22) code, with the ultrasoft pseudopotential plane-wave method. In order to determine the true ground state, we have considered four different cases. These are NM, FM, and the two different AF spin configurations. The first one of the AF configurations is AF1 (checkerboard AF), where the nearest-neighbor spins of Fe atoms are antiparallel to each other. The second AF configuration is AF2 (stripe AF), where the Fe spins along the square diagonal are aligned antiferromagnetically. This is the stripe phase, which was first predicted from the Fermi-surface nesting.[23,24] After carefully checking the convergence with respect to the cutoff energy and the number of *k* points, we adopt a cutoff energy of 30 Ry for all the states and generated *K* points using the Monkhorst-Pack scheme with $12\times12\times4$ grids for the NM, FM, and AF1 states and $8\times8\times4$ grids for the AF2 state.

By fixing the lattice constants to the experimental ones, we optimized the atomic position by minimizing the force on atoms, where the GGA to exchange-correlation potential in the Perdew-Burke-Ernzerhof (PBE) form was used.[25] For the

TABLE I. The optimized atomic positions in cell of tetragonal (space group $P4/nmm$, NM phase), with experimental lattice constants. The atomic coordinates from experiment and optimized by Shein are also listed for comparison. We only list the atomic coordinates in c axis because the atomic coordinates in a axis and b axis are determined by the symmetry.

$(Sr_2ScO_3)_2Fe_2As_2$ (a=4.045 Å and c=15.695 Å)				$(Sr_2VO_3)_2Fe_2As_2$ (a=3.930 Å and c=15.666 Å)	
Atom (site)	z	Opti (Ref. 21)	Expt. (Ref. 20)	Atom (site)	z
Sr(2c)	0.3172	0.3176	0.3113	Sr(2c)	0.3183
Sr(2c)	0.0860	0.0870	0.0847	Sr(2c)	0.0863
Sc(2c)	0.8052	0.8042	0.8071	V(2c)	0.8011
O1(4f)	0.2170	0.2179	0.2142	O1(4f)	0.2068
O2(2c)	0.9325	0.9325	0.9301	O2(2c)	0.9268
Fe(2b)	0.5000	0.5000	0.5000	Fe(2b)	0.5000
As(2c)	0.5760	0.5778	0.5854	As(2c)	0.5808

FM and AF1 states, we used the same unit cell as that of NM state while we used the $\sqrt{2}\times\sqrt{2}$ supercell for the AF2 state. In the calculations of magnetic states, such as FM, AF1, and AF2 states, the atomic coordinates are the same as those used in the NM state.

III. RESULTS AND DISCUSSION

A. Nonmagnetic state

The atomic positions for both $(Sr_2ScO_3)_2Fe_2As_2$ and $(Sr_2VO_3)_2Fe_2As_2$ are optimized with their lattice constants fixed to the experimental values. Both the lattice constants and the atomic position are presented in Table I, where we also list the experimental atomic positions and the optimized ones by Shein[21] for comparison. From Table I, we can see that our optimized atomic positions of $(Sr_2ScO_3)_2Fe_2As_2$ reasonably agree with Shein's[21] results. For $(Sr_2ScO_3)_2Fe_2As_2$, our optimized FeAs bond length is 0.078 Å shorter than the experimental one. In LaOFeAs, Yin[26] preformed GGA calculations and found the optimized FeAs bond length is 0.1 Å shorter than the experimental one. Such difference has been explained by the effect of spin[26,27] and orbital fluctuation.[28] The difference between optimized and experimental FeAs bond length in $(Sr_2ScO_3)_2Fe_2As_2$ is smaller than that in LaOFeAs and $BaFe_2As_2$, which indicates that the spin and orbital fluctuations in $(Sr_2ScO_3)_2Fe_2As_2$ is suppressed by the larger d_{FeAs}.

Let us first study the electronic structure of the NM state because it has been confirmed that above T_C the normal state

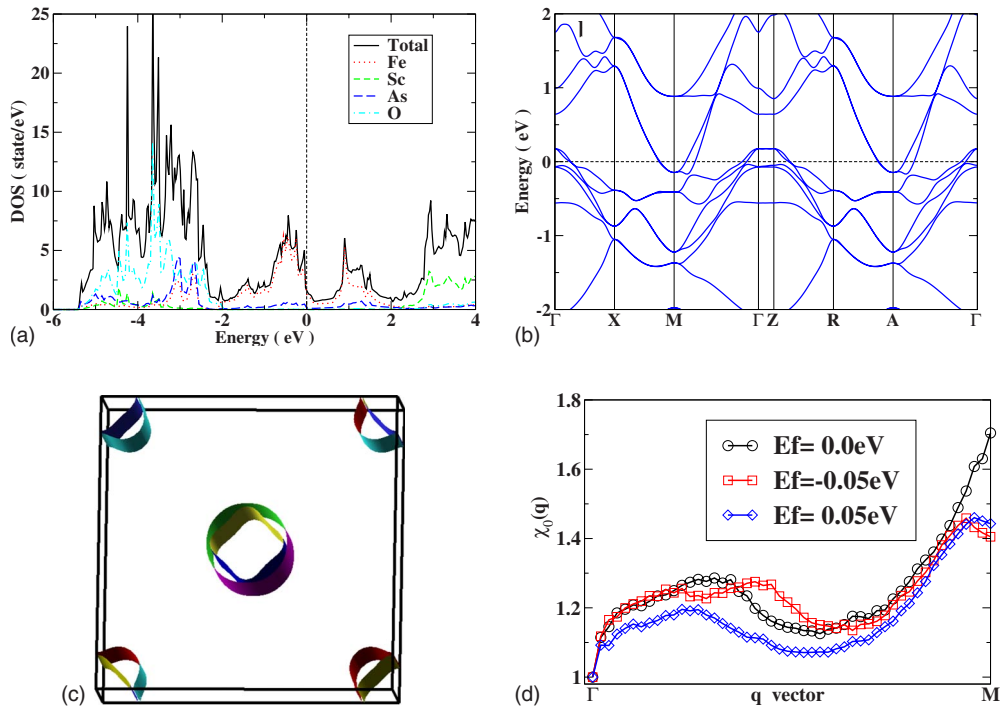

FIG. 1. (Color online) (a) The density of state, (b) band structure, (c) Fermi surface, and calculated Lindhard response function $\chi(q)$ of $(Sr_2VO_3)_2Fe_2As_2$ in the nonmagnetic state.

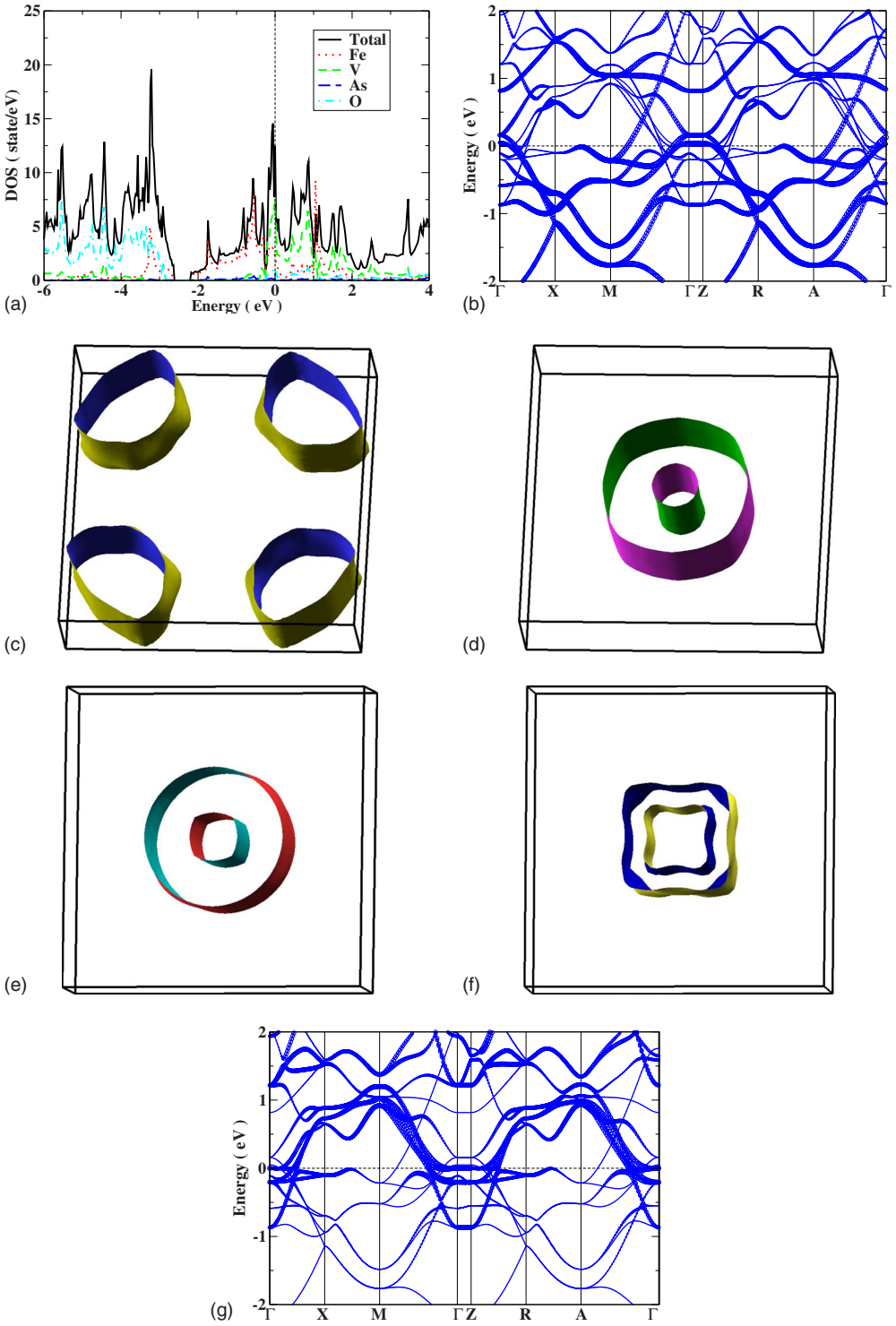

FIG. 2. (Color online) (a) The density of state, [(b) and (c)] band structure, and [(d1)–(d4)] Fermi surface of $(Sr_2VO_3)_2Fe_2As_2$ in the nonmagnetic state. We plot the fat bands, where the symbol size corresponds to the projected weight of Bloch states onto the (b) Fe 3*d* states and (c) V 3*d* states.

is paramagnetic metal in LaOFeAs and $BaFe_2As_2$. The density of state, band structure, FS and calculated Lindhard response function $\chi(q)$ of $(Sr_2ScO_3)_2Fe_2As_2$ in the nonmagnetic state are presented in Figs. 1(a)–1(d), respectively. In Fig. 1(a), the states between −2 and +2 eV are mostly derived from Fe 3*d* states, just below which (from −6 to −2 eV) are the states of O *p* and As *p*. The *p*-*d* hybridization between O and Fe is negligible while that hybridization between As and Fe is sizable. Such results are similar to those of $LnFeAsO_{1-x}F_x$ (Ref. 23) and $A_{1-x}K_xFe_2As_2$.[10] The density of states (DOS) at Fermi level $N(E_f)$ is 1.64 eV^{-1} per formula unit. From the $N(E_f)$, the calculated bare susceptibility and the specific-heat coefficient are 5.3×10^{-5} emu/mol and 4.1 mJ/(K^2 mol), respectively, which are smaller than those

TABLE II. The energy (per formulas) of FM, AF1, and AF2 states with respect to NM state (in eV).

Sample	NM	FM	AF1	AF2
Sc-42622	0.0	0.0	0.0918	0.2216
V-42622	0.0	0.6258	0.6717	0.373

in LaOFeAs (Ref. 23) [$\chi_0=8.5\times10^{-5}$ emu/mol and $\gamma_0=6.5$ mJ/(K^2 mol)].

The band structure and FS of $(Sr_2ScO_3)_2Fe_2As_2$ are presented in Figs. 1(b) and 1(c), respectively, which show two holelike FS circling around Γ and two electronlike FS circling around M. By shifting the FS around Γ to M, i.e., by a vector $q=(\pi,\pi,0)$, the holelike FS will largely overlap with the electronlike FS, suggesting significant nesting effect. Such nesting effect can be quantitatively estimated by calculating the Lindhard response function $\chi_0(q)$ as shown in Fig. 1(d), where $\chi_0(q)$ is strongly peaked at M point for undoped compound, and it is obviously suppressed and become slightly incommensurate for both electron doping and hole doping. The author[15] did not find the spin-density wave (SDW) state maybe because there were some impurities or oxygen deficiencies in their sample (they also mentioned this possibility in their following work[20]). The suppression of $\chi_0(q)$ with electron doping can be understood with "rigid" band shifting. Because the electron doping shifts the Fermi level up, which tends to reduce the size of the holelike FS and enlarge the electronlike FS, and it reverses with hole doping. The existence of strong nesting effect would suggest that certain kinds of ordering, such as charge-density wave or SDW,[23,24] may develop at low temperature in the undoped compound, just like LaOFeAs.[23,24,29] So we will study the electronic structure of $(Sr_2ScO_3)_2Fe_2As_2$ in the stripe AF ordering in the next section.

The DOS, band structure, and FS of $(Sr_2VO_3)_2Fe_2As_2$, shown in Figs. 2(a)–2(d), are significantly different from those of $(Sr_2ScO_3)_2Fe_2As_2$. We can see that the states between −2 and +2 eV are mainly derived from not only Fe 3*d* states but also V 3*d* states. At the Fermi level, the DOS of V 3*d* states is even higher than that of Fe 3*d* states. From −6 to −2 eV, the states are mainly derived from O *p* and As *p*, which is similar to $(Sr_2ScO_3)_2Fe_2As_2$. The *p*-*d* hybridization between O and V is greater than that between As and Fe. The DOS at Fermi level $N(E_f)$ is 12.88 eV^{-1}, which will induce magnetic unstable, according to the Stoner criteria.[30] From the $N(E_f)$, we calculated the bare susceptibility and specific-heat coefficient are 4.1×10^{-4} emu/mol and 30.9 mJ/(K^2 mol), respectively. The band structure and FS are more complex than those of $(Sr_2ScO_3)_2Fe_2As_2$. In $(Sr_2ScO_3)_2Fe_2As_2$, all the FS are derived from Fe 3*d* states while in $(Sr_2VO_3)_2Fe_2As_2$ the holelike FS [Fig. 2(d)1] is mostly derived from Fe 3*d* states and the other three electronlike FS [Figs. 2(d)2–2(d)4], circling around Γ point, are mostly derived from both Fe 3*d* and V 3*d* states. From the fat bands [Figs. 2(b) and 2(c)], we found a very interesting result that every electronlike FS had two sheets, the inner sheet coming from Fe 3*d* states and the outer sheet coming from V 3*d* states. The band structure and FS indicate that not only Fe 3*d* states but also V 3*d* states may play important roles in the superconductivity. From the volumes enclosed by the holelike and electronlike Fermi surfaces, we find that the hole and electron carrier density are about 1.36×10^{21}/cm^3 and 1.73×10^{21}/cm^3, respectively. Such result is consistent with Zhu's report,[20] where they found the carrier is electron rather than hole at all the measured temperatures.

TABLE III. The moment (μ_B) of Sc, Fe, and V in the FM, AF1, and AF2 states.

Sample	Atom	FM	AF1	AF2
Sc-42622	Sc	0.0	0.0	0.0
	Fe	0.0	1.63	1.88
V-42622	V	1.51	1.50	1.24
	Fe	0.03	1.23	1.48

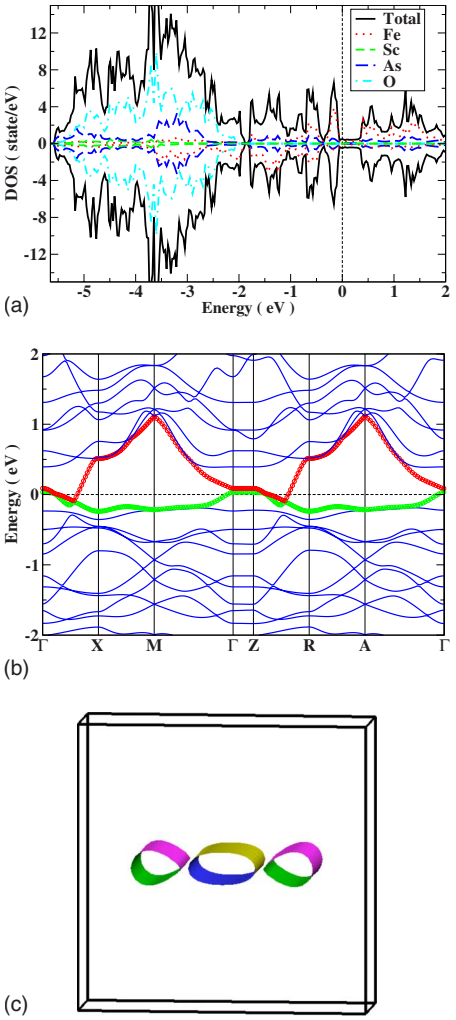

FIG. 3. (Color online) (a) The density of state, (b) band structure, and Fermi surface of $(Sr_2ScO_3)_2Fe_2As_2$ in the AF2 state.

B. Antiferromagnetic state

As mentioned in the introduction, Shein and Ivanovskii[21] had studied the electronic structure of $(Sr_2ScO_3)_2Fe_2As_2$ and

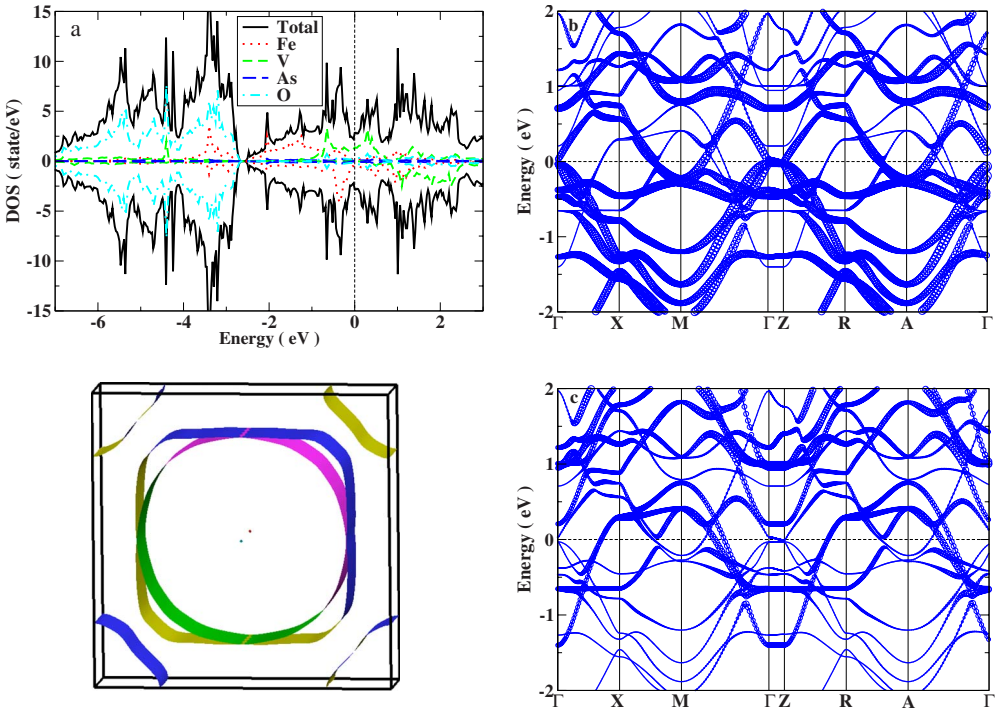

FIG. 4. (Color online) (a) The density of state, [(b) and (c)] band structure, and (d) Fermi surface of $(Sr_4V_2O_6)Fe_2As_2$ in AF1 state. We plot the fat bands, where the symbol size corresponds to the projected weight of Bloch states onto the (b) Fe 3*d* states and (c) V 3*d* states.

$(Sr_2VO_3)_2Fe_2As_2$ by the first-principles FLAPW-GGA calculations. They found nonmagnetic $(Sr_2ScO_3)_2Fe_2As_2$ was formed from nonmagnetic conducting $[Fe_2As_2]$ layers and insulating $(Sr_2ScO_3)_2$ blocks while $(Sr_2VO_3)_2Fe_2As_2$ was constructed of nonmagnetic conducting $[Fe_2As_2]$ layers and magnetic half-metallic $[Sr_4V_2O_6]$ blocks.[21] That is, to say, they found the ground states of $(Sr_2ScO_3)_2Fe_2As_2$ and $(Sr_2VO_3)_2Fe_2As_2$ are nonmagnetic state and ferromagnetic state, respectively. However, they only involved the nonmagnetic and ferromagnetic states, without the antiferromagnetic state in their calculations. In order to determine the true ground state, we have calculated the total energies of $(Sr_2ScO_3)_2Fe_2As_2$ and $(Sr_2VO_3)_2Fe_2As_2$ in four different magnetic states, such as NM, FM, AF1, and AF2. The total energies (per formulas) of FM, AF1, and AF2 states (with respect to NM state) are presented in Table II. We can see the ground states of $(Sr_2ScO_3)_2Fe_2As_2$ and $(Sr_2VO_3)_2Fe_2As_2$ are AF2 and AF1, respectively. For $(Sr_2ScO_3)_2Fe_2As_2$, the ground-state AF2 is 0.22 eV more favorable than NM state, which can be understood from the FS nesting effect. Such nesting effect induced SDW has been well discussed in LaOFeAs and $BaFe_2As_2$.[23,24] However, in $(Sr_2VO_3)_2Fe_2As_2$, the FS nesting effect is disappeared and the ground state is AF1. In Table III, we present the magnetic moments of Sc, Fe, and V atoms in the FM, AF1, and AF2 states for both $(Sr_2ScO_3)_2Fe_2As_2$ and $(Sr_2VO_3)_2Fe_2As_2$. For $(Sr_2ScO_3)_2Fe_2As_2$, the magnetic moment of Sc is zero in all the magnetic state while the magnetic moment of Fe is $1.88\mu_B$ in the ground state (AF2). Our FM results (converged to the NM state) are consistent with Shein's,[21] where they started calculation from FM state for $(Sr_2ScO_3)_2Fe_2As_2$ but the magnetic moment of Fe converges to zero, so they drew the conclusion that the ground state was NM state. However, when we include two types of antiferromagnetic states, the ground state is AF2 state. In $(Sr_2VO_3)_2Fe_2As_2$, the FS nesting effect absents and the ground state is AF1, where the magnetic moments of V and Fe are $1.50\mu_B$ and $1.23\mu_B$, respectively.

In order to understand the ground state of $(Sr_2ScO_3)_2Fe_2As_2$, we show the total and projected density of states, band structure, and FS of AF2 state in Fig. 3. Let us first focus on the states between −2 and +2 eV because the property of the compound is mainly determined by the DOS near Fermi level. It is obviously that this part of DOS are mostly derived from Fe 3*d* states, just below which (from −6 to −2 eV) are the states of O *p* and As *p*, which is similar to the results of NM state. However, there is an important difference that the Fermi level locates at the "pseudogap," which may explain why the AF2 state is more stable than the other states. Unlike nonmagnetic state, there are only two Fermi-surface sheets, one small hole cylinder circling along Γ-Z line and the other small electron pocket locating at the middle of Γ-X line. From the volumes enclosed by these Fermi surfaces, the calculated hole and electron carrier densities are about $1.02\times10^{20}/\mathrm{cm}^3$ and $1.30\times10^{20}/\mathrm{cm}^3$, respectively.

Figure 4 shows the total and projected density of states, band structure, and FS of $(Sr_2VO_3)_2Fe_2As_2$ in AF1 state. From −2 to +1 eV, the states are mostly derived from both Fe 3*d* and V 3*d* states, just below which (from −6 to −2 eV) are the states of O *p* and As *p*. There are three bands crossing Fermi level. The largest cylinder FS circling along Γ-Z and the very small pocket locating at Z point are electronlike FS. For the large holelike FS, it has two sheets, one circling along Γ-Z line, the other circling along M-A line (at the corner of Brillouin zone). From the volumes enclosed by these Fermi surfaces, the calculated hole and electron carrier

densities are about $8.40\times10^{20}/\mathrm{cm}^3$ and $8.37\times10^{20}/\mathrm{cm}^3$, respectively. From the fat bands, we can see that the two cylinder Fermi surfaces, circling along Γ-Z line, are mostly derived from V 3*d* states while the sheet centered along M-A line is mostly derived from Fe 3*d* states. Combining Fig. 2 with Fig. 4, it obviously shows that the V 3*d* states show great contribution to the Fermi surface in both NM and AF1 states. It means that the V 3*d* states may play important roles in the superconductivity of $(Sr_2VO_3)_2Fe_2As_2$.

In summary, by the first-principles calculations, we have studied the electron structure of $(Sr_2ScO_3)_2Fe_2As_2$ and $(Sr_2VO_3)_2Fe_2As_2$. We find that the Fermi-surface nesting induced stripe antiferromagnetic state (AF2) is the ground state of $(Sr_2ScO_3)_2Fe_2As_2$ while the ground state of $(Sr_2VO_3)_2Fe_2As_2$ is the checkerboard antiferromagnetic state (AF1). Both band structure and Fermi surface of $(Sr_2ScO_3)_2Fe_2As_2$ are similar to those of LaOFeAs while electronic structure of $(Sr_2VO_3)_2Fe_2As_2$ shows significant difference. The V 3*d* states show great contribution to the states at Fermi level, which implies that the V 3*d* states may play important roles for the superconductivity in $(Sr_2VO_3)_2Fe_2As_2$.

ACKNOWLEDGMENT

The authors acknowledge the supports from NSF of China (Grant No.10674042).

[1] Y. Kamihara, T. Watanabe, M. Hirano, and H. Hosono, J. Am. Chem. Soc. **130**, 3296 (2008).
[2] X. H. Chen, T. Wu, G. Wu, R. H. Liu, H. Chen, and D. F. Fang, Nature (London) **453**, 761 (2008).
[3] G. F. Chen, Z. Li, D. Wu, G. Li, W. Z. Hu, J. Dong, P. Zheng, J. L. Luo, and N. L. Wang, Phys. Rev. Lett. **100**, 247002 (2008).
[4] Z. A. Ren, J. Yang, W. Lu, W. Yi, X. L. Shen, Z. C. Li, G. C. Che, X.-L. Dong, L. L. Sun, F. Zhou, and Z. X. Zhao, EPL **82**, 57002 (2008).
[5] R. Zhi-An, L. Wei, Y. Jie, Y. Wei, S. Xiao-Li, Zheng-Cai, C. Guang-Can, D. Xiao-Li, S. Li-Ling, Z. Fang, and Z. Zhong-Xian, Chin. Phys. Lett. **25**, 2215 (2008).
[6] M. Rotter, M. Tegel, D. Johrendt, I. Schellenberg, W. Hermes, and R. Pöttgen, Phys. Rev. B **78**, 020503(R) (2008).
[7] M. Rotter, M. Tegel, and D. Johrendt, Phys. Rev. Lett. **101**, 107006 (2008).
[8] K. Sasmal, B. Lv, B. Lorenz, A. M. Guloy, F. Chen, Y. Y. Xue, and C. W. Chu, Phys. Rev. Lett. **101**, 107007 (2008).
[9] H. Ding, P. Richard, K. Nakayama, K. Sugawara, T. Arakane, Y. Sekiba, A. Takayama, S. Souma, T. Sato, T. Takahashi, Z. Wang, X. Dai, Z. Fang, G. F. Chen, J. L. Luo and N. L. Wang, EPL **83**, 47001 (2008).
[10] G. Xu, H. J. Zhang, X. Dai, and Z. Fang, EPL **84**, 67015 (2008).
[11] G. Wu, R. H. Liu, H. Chen, Y. J. Yan, T. Wu, Y. L. Xie, J. J. Ying, X. F. Wang, D. F. Fang, and X. H. Chen, EPL **84**, 27010 (2008).
[12] J. H. Tapp, Z. J. Tang, B. Lv, K. Sasmal, B. Lorenz, Paul C. W. Chu, and A. M. Guloy, Phys. Rev. B **78**, 060505(R) (2008).
[13] X. C. Wang, Q. Q. Liu, Y. X. Lv, W. B. Gao, L. X. Yang, R. C. Yu, F. Y. Li, and C. Q. Jin, Solid State Commun. **148**, 538 (2008).
[14] F. C. Hsu, J. Y. Luo, K. W. Yeh, T. K. Chen, T. W. Huang, P. M. Wu, Y. C. Lee, Y. L. Huang, Y. Y. Chu, D. C. Yan, and M. K. Wu, Proc. Natl. Acad. Sci. U.S.A. **105**, 14262 (2008).
[15] X. Zhu, F. Han, G. Mu, B. Zeng, P. Cheng, B. Shen, and H. H. Wen, Phys. Rev. B **79**, 024516 (2009).
[16] H. Ogino, Y. Matsumura, Y. Katsura, K. Ushiyama, S. Horii, K. Kishio, and J. Shimoyama, arXiv:0903.3314 (unpublished).
[17] H. Ogino, Y. Katsura, S. Horii, K. Kishio, and J. Shimoyama, Supercond. Sci. Technol. **22**, 085001 (2009).
[18] G. F. Chen, T. L. Xia, P. Zheng, J. L. Luo, and N. L. Wang, Supercond. Sci. Technol. **22**, 072001 (2009).
[19] Y. L. Xie, R. H. Liu, T. Wu, G. Wu, Y. A. Song, D. Tan, X. F. Wang, H. Chen, J. J. Ying, Y. J. Yan, Q. J. Li, and X. H. Chen, EPL **86**, 57007 (2009).
[20] X. Y. Zhu, F. Han, G. Mu, P. Cheng, B. Shen, B. Zeng, H. H. Wen, Phys. Rev. B **79**, 220512(R) (2009).
[21] I. R. Shein and A. L. Ivanovskii, arXiv:0903.4038 (unpublished); arXiv:0904.0117 (unpublished); and arXiv:0904.2671 (unpublished).
[22] Z. Fang and K. Terakura, J. Phys.: Condens. Matter **14**, 3001 (2002).
[23] D. J. Singh and M. H. Du, Phys. Rev. Lett. **100**, 237003 (2008); G. Xu, W. Ming, Y. Yao, X. Dai, S.-C. Zhang, and Z. Fang, EPL **82**, 67002 (2008).
[24] J. Dong, H. J. Zhang, G. Xu, Z. Li, G. Li, W. Z. Hu, D. Wu, G. F. Chen, X. Dai, J. L. Luo, Z. Fang, and N. L. Wang, EPL **83**, 27006 (2008); C. de la Cruz, Q. Huang, J. W. Lynn, Jiying Li, W. Ratcliff II, J. L. Zarestky, H. A. Mook, G. F. Chen, J. L. Luo, N. L. Wang, and Pengcheng Dai, Nature (London) **453**, 899 (2008).
[25] J. P. Perdew, K. Burke, and M. Ernzerhof, Phys. Rev. Lett. **77**, 3865 (1996).
[26] Z. P. Yin, S. Lebegue, M. J. Han, B. P. Neal, S. Y. Savrasov, and W. E. Pickett, Phys. Rev. Lett. **101**, 047001 (2008).
[27] S. Lebègue, Z. P. Yin, and W. E. Pickett, New J. Phys. **11**, 025004 (2009).
[28] G. T. Wang, Y. M. Qian, G. Xu, X. Dai, and Z. Fang, arXiv:0903.1385 (unpublished).
[29] F. Ma and Z. Y. Lu, Phys. Rev. B **78**, 033111 (2008).
[30] E. C. Stoner, Proc. R. Soc. London, Ser. A **165**, 372 (1938).